International Journal of Fluid Power, 2015
Vol. 16, No. 1, 1–10, http://dx.doi.org/10.1080/14399776.2015.1006979

Taylor & Francis
Taylor & Francis Group

Axial piston pumps slippers with nanocoated surfaces to reduce friction

G. Rizzo[a], G.P. Massarotti[a], A. Bonanno[a]*, R. Paoluzzi[a], M. Raimondo[b], M. Blosi[b], F. Veronesi[b], A. Caldarelli[b] and G. Guarini[b]

[a]*Institute for Agricultural and Earthmoving Machines – IMAMOTER – C.N.R., via Canal Bianco 28, 44124 Ferrara, Italy;*
[b]*Institute of Science and Technology for Ceramics – ISTEC – C.N.R., via Granarolo 64, 48018 Faenza, Italy*

(*Received 12 September 2014; accepted 9 January 2015*)

This paper shows the experimental results obtained using a nanocoating (developed by ISTEC-C.N.R.) applied to the slippers of an axial piston pump to reduce the friction losses in order to improve the pump overall efficiency map. It is well known that the mechanical power losses in a hydraulic pump come from the friction between parts in relative motion. The need to provide, especially at low rotational speed, hydrodynamic lift causes power losses in terms of volumetric and mechanical efficiency, due to the contrasting need to increase leakage to provide lubrication and to keep a minimum clearance in meatus to limit the volumetric losses. The application of special surface treatments have been exploited in pioneering works in the past, trying different surface finishing or adding ceramic or heterogeneous metallic layers, but the potential of structured coatings at nanoscale, with superhydrophobic and oleophobic characteristics, has never been exploited. Using a dedicated test rig developed at IMAMOTER-C.N.R., able to ensure hydrostatic working condition during the mutual rotation between the slippers and the swash plate, the functional performance of the nanocoated slippers' surface have been studied. In the first part of the paper, the functionalization method is presented; in the second part, a comparison between the experimental performances of coated and uncoated surfaces is showed.

Keywords: superoleophobic; nanocoating; slipper; friction

1. Introduction

Axial piston pumps and motors are widely used in heavy-duty applications and play a fundamental role in hydrostatic and power-split drives (Paoluzzi *et al*. 1996). The improvement, albeit marginal, in overall efficiency of these components may significantly impact the global efficiency of the machine. Friction between slipper and swash plate is a functional key in the axial piston pump, especially when the pump (at low rotational speed or at partial displacement) works in the critical areas where the efficiency is low, as showed in Figure 1.

There are several challenging issues associated with the pump, such as conflicts between lubrication and wear, and between sealing and leakage. Particularly, in an axial piston pump, slipper and swash plate can form a key friction pair, where the above conflicts exist and may result in significant influences on the pump's performance.

Hydrostatic slipper bearing is an effective way to maintain a fluid film between slipper and swash plate that slide on one another, and thereby mitigating surface-to-surface direct contact.

In this context, it is useful to introduce the concept of wettability (Miwa *et al*. 2000), which is one of the most important properties of solid surfaces when interaction with fluids occur. The main factors influencing wettability are related to roughness factors and, depending on the physical properties of fluids (particularly, surface tension), the energy of surfaces and their polar/disperse components. A significant improvement of repellence toward liquids (water or low-surface tension liquids and fluids) is achieved when roughness values fall in the nanometric range, so that inhomogeneous wetting mechanisms are working (Cassie and Baxter 1944, Yong and Bhushan 2006), and when the surface energy is kept as low as possible (Khoo and Tseng 2008). Generally speaking, wettability can be modulated by a combined approach suitable to control both microstructural and chemical features of surfaces.

The degree of hydrophobicity (repellence against water) or oleophobicity (repellence against oils and lubricants) can be easily quantified by the determination of the contact angle which the liquid droplet forms on the material surface. When a liquid droplet is spreading out on a surface, the value of the contact angle is very low and there is a great affinity of that material with the given liquid and, hence, a low ability of repelling it (hydrophilic or oleophilic behavior). The greater the increase in the contact angle over the conventional limit of 90°, the greater the repellence ability and the lowest the interactions between the surface and the liquid during wetting (Figure 2). In the literature, surfaces presenting contact angles with water greater than 150° are referred to as *superhydrophobic*, while those presenting contact angle with oil greater than and 120°–130° are referred to as *superoleophobic.* Superoleophobic performances

*Corresponding author. Email: a.bonanno@imamoter.cnr.it

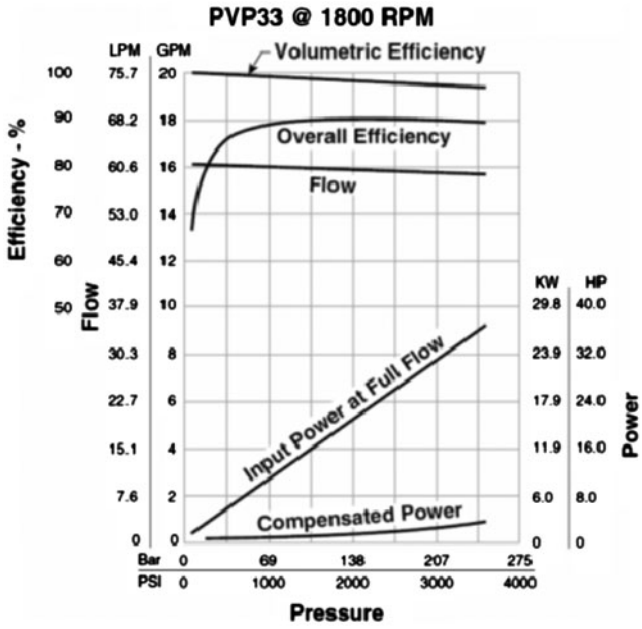

Figure 1. efficiency chart of a piston pump.
Source: Parker Hannifin Corporation.

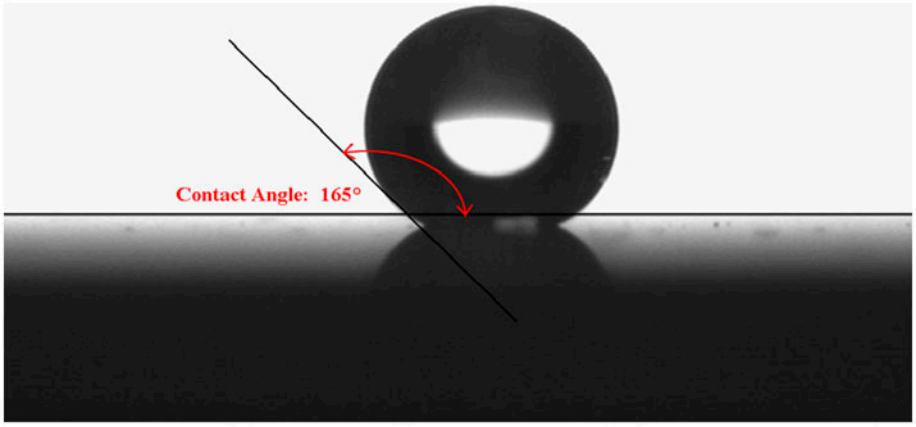

Figure 2. Hydrophobic behavior and contact angle.
Source: Laurel Products, LLC.

described in the literature (Tuteja *et al*. 2007, Bhushan 2011, Wilson and Hayme 2009) are generally characterized by surface energy values <5 mN/m. In fact, due to the low surface tension of oils and alkanes, the difference between the surface energy value of the solid and the surface tension of the liquid to be repelled need to be kept as large as possible. This implies that a significant reduction of the surface energy value of the solid is mandatory to reduce wetting and obtain oleophobicity or superoleophobicity.

Many studies on hydrostatic thrust bearing in hydraulic axial piston equipment were carried out through considering multiple impact factors, such as operating conditions, geometric parameters, and matching materials. Kazama and Yamaguchi (1993a, 1993b) focused on reasonable design criteria for optimum sizes of the bearing and the seal parts of the hydraulic equipment under the conditions of concentric loads and steady state. In particular, they studied a flat oil-lubricated metallic slipper bearing. Mixed lubrication characteristics of hydrostatic thrust bearings were examined experimentally in another research of the same author (Kazama and Yamaguchi 1995). A significant agreement exists between the experimental outputs and the theoretical results from a mixed lubrication model proposed.

Pang *et al*. (1993) studied the lubrication condition between the slipper and the oblique plate of a high pressure pump that affects its operating life. They investigated the oil film pressure distribution and load characteristics by considering the pressure–viscosity effect of the lubricant, the pressure–elasticity effect of the lubricating surface, and the properties of dynamic stiffness in the oil film.

Koc *et al*. (1992) and Hooke (1989) carried out an experimental and theoretical investigation of the effects of deformation in slipper pad, clamping ratio, and orifice size on the load-carrying capacity of hydrostatic thrust bearing under a low-speed condition in axial piston pumps and motors. They concluded that polishing of the running face to a slightly convex form appeared to be essential for successful operation under all conditions; the orifice in under-clamped slippers could increase the clearance and destabilize the slipper, which would result in the slipper becoming sensitive to the effect of tilting couples; the design for over-clamped slippers seemed to depend on the precise value of the clamping ratio and the width of the slipper land. In other research (Li and Hooke 1991), friction of water-based slippers was measured. The results were consistent with the clearances predicted by using the model developed for oil-based slippers, although the clearances are now typically below 1 μm.

Up to date, at our knowledge, no attempts have been done with the aim of improving lubrication between slipper and swash plate by treatments of the involved surfaces and application of structured coatings in helping the friction reduction.

In this context, the functionalization of slippers, whose surface energy is generally lower than 3mN/m, revealed to be successful leading to an improvement of materials' efficiency through a significant reduction of the friction coefficient (Bhushan 2011, Zhou *et al*. 2011, Wu *et al*. 2014).

In the last years, using metals, alloys or polymers as substrates, many different strategies have been developed to design functional materials with enhanced repellence to polar or non-polar fluids. However, the application of surface functionalization in the field of fluid power design is a completely new area of application. The engineering of textured surfaces that repel a range of polar and non-polar liquid through appropriate combination of local structural features and chemical modification is still a hard task. No reference exists in literature, in practice or in patent databases directly addressing the potential benefits to hydraulic pumps and motors of the approach proposed. The problem of slipper behavior in swash plate axial piston pumps is addressed by several authors (Kumar *et al*. 2009, Manring *et al*. 2004), and generally tackled with experimental measures or application of CFD codes using the simplified lubrication Reynolds equation or a full 3D Navier–Stokes approach (Kumar *et al*. 2009). In spite of the complex interaction between boundary layer extension and flow motion character (either turbulent or laminar) all models ground their base on the existence of a no-slip boundary condition between fluid and solid.

The work here presented aims at removing this assumption, exploiting the potential of lubricated microchannel with a slip length of the same order of magnitude of the geometrical interface (Li *et al*. 2009, Liu *et al*. 2010, Yao *et al*. 2004, Yu and Wei 2006). Another important issue concerns the dynamic behavior of surfaces, which is related to their ability to promote fluid motion after the application of an external force, affecting the development of fluid-caused drag and lift forces. These aspects have been investigated and described only in very few scientific papers in the laminar field of motion (Iwatsu *et al*. 1993) and in turbulent conditions (Martell *et al*. 2010, Rothstein Jonathan 2010) none of the reported studies, however, apply the concept to real cases in operation and no documentation exists in linking the proven drag and friction reduction effect to the impact on actual components efficiency.

2. The functional layer

The design and synthesis of hybrid organic–inorganic coatings – with a tailored nanostructure and a controlled chemistry – are able to significantly reduce the wettability of metals and alloys against fluids have been developed and patented by ISTEC-C·N.R (Patent 1 2011, Patent 2 2012, Raimondo 2012). The coating composition is fully compatible from the chemical point of view with the component to be functionalized. In many cases, experimental routes to oleophobic metals have not been successfully pursued being particularly complex and expensive, and therefore not suitable to be applied on an industrial scale. In this context, precursors of the organic–inorganic coatings have been obtained in the form of stable nanosuspensions in water by a sol–gel approach (Ma *et al*. 2012, Raimondo 2012, Raimondo *et al*. 2014), getting a high control degree on phases, particle size (average particle dimensions of about 40 nm), and composition. The details of synthesis and deposition methodologies are presented elsewhere (Raimondo *et al*. 2014, Tadanaga *et al*. 1997)

Nanostructured coatings on pristine sample (Figure 3) with a thickness in the 200–500 nm range were obtained by simple dip coating technology (Raimondo *et al*. 2014).

3. Samples characterization

The functional surfaces treated as described were subjected to several tests to verify their static contact angle with water (WCA); dynamic contact angle and hysteresis

Figure 3. Pristine sample made in $CuZn_40Al_2$ alloy.

with water (CAH); contact angle with lubricant (CA), particularly with Arnica 46 representative of the oils used in axial pumps and surface energy (SE). The slippers are made in $CuZn_40Al_2$ alloy, the inner hole radius (r_0) is 0.5 mm, the slipper inner radius (R_1) = 9.25 mm, and the slipper outer radius (R_2) is 14.15 mm.

Since the slippers present a complex shape and were dip coated by immersion in the nanosuspension in two different directions (along vertical and horizontal axis, respectively), four different areas of the samples were characterized in order to evaluate the treatment's homogeneity. However, for a better statistical significance, a greater number of analyses were done on the whole upper face of the sample, inside and outside the crown (zone 1) (Figure 4), which is the main contact area between the slipper and the swash plate.

All measurements were performed on functionalized samples, comparing the data with those of the uncoated, reference ones (R). Water static contact angle measurements (WCA) were performed on two treated samples ("1 horizontal" and "2 vertical") and two untreated samples (UT) taken as references (one non-sandblasted and one sandblasted). Measurements were performed according to the sessile drop method, laying a 1 μL water drop on the sample surface. Contact angles were measured with DataPhysics OCA 15Plus tensiometer equipped with a CCD camera. WCA values on the different areas of the samples are listed in Table 1.

From WCA data, the following information can be obtained:

- Sandblasting procedures of samples surface promote an increasing of the starting roughness and, then, an increasing of the final WCA values due to a better adhesion of the coating.
- The hybrid organic–inorganic coating is able to promote a high degree of hydrophobicity, switching the contact angles values from hydrophilic to typically (super)hydrophobic ones.
- Dipping the sample along the vertical axis provides a higher values of WCA in zone 1 (158.8°) than dipping the sample along the horizontal axis (142.6°).

WCAs measured on other zones are less significant either because the surface is curved (zones 2 and 3) or very restricted (zone 4), making the measurement difficult and not reliable.

On zone 1 of treated samples, the water contact angle hysteresis (CAH) was determined by the needle-in technique with droplet volume of 2 μL. The smaller the hysteresis value, the better surface ability to promote the drop sliding and, then, the more efficient the dewetting phenomenon will be. CAH values measured on coated samples are listed in Table 2.

The sample dipped along the vertical axis proved to be more performing also in terms of hysteresis. Measurements of diiodomethane static contact angle were performed on zones 1 and 2 of the treated samples and of an untreated, sandblasted sample. Diiodomethane has a surface tension of 50.8 mN/m; using the contact angle values obtained with water and diiodomethane it is possible to calculate the surface energy of different zones by the Owens–Wendt–Rabel–Kaelble algorithm (Table 3).

The treatment clearly reduces surface energy (down to values close to zero) with respect to the untreated sample; furthermore, the lowest SE value (0.47 mN/m) was observed on zone 1 of the sample dipped with vertical axis. Low surface energy is the key parameter, together with surface nanostructure, to obtain oleophobicity (Martell *et al*. 2010, Rothstein Jonathan 2010, Raimondo and Blosi 2011).

The characterization clearly shows that the highest repellence and the lowest values of surface energy are obtained when the vertical conformation of the sample during dipping is adopted. In this case, the contact angle with the lubricant oil Arnica 46 (surface tension 29.4 mN/m) was measured. As a reference, same measurements were performed on an untreated, sandblasted sample (Table 4).

The treatment radically modifies the wettability of the sample toward the lubricant oil: from an extremely oleophilic behavior (CA equal to 17°, denoting *affinity* of the slipper surface for the lubricant) to a quite strong oleophobicity (CA equal to 124°, denoting *repellence* of the slipper surface toward the lubricant).

4. Performance evaluation on test bench

It is not so easy to analyze the hydrostatic working condition directly using a piston pump. The paper is focused

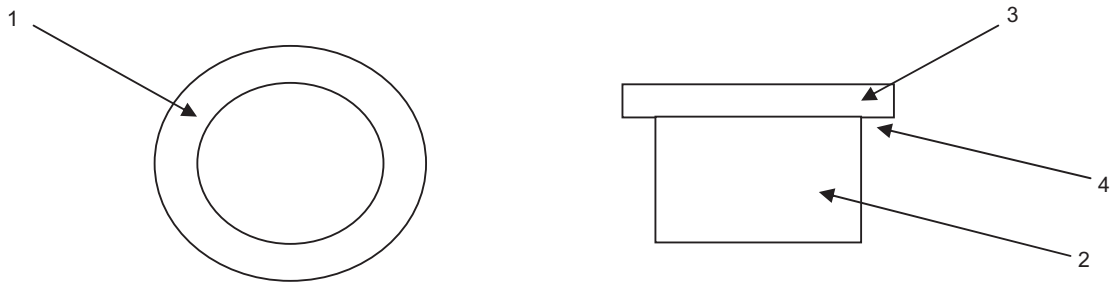

Figure 4. Mapping of the different zones of the slippers where characterizations were performed.

Table 1. WCA values in different areas of the samples.

	WCA (°)			
Sample	Zone 1	Zone 2	Zone 3	Zone 4
R no sandblasted	74.8 ± 1.0	88.9 ± 1.1	–	–
UT sandblasted	108.5 ± 2.5	109.1 ± 4.0	105.4 ± 2.0	98.0 ± 1.5
1 horizontal	142.6 ± 2.6	122.0 ± 5.1	120.8 ± 2.7	124.4 ± 3.0
2 vertical	158.8 ± 2.8	123.5 ± 3.0	134.7 ± 1.6	112.2 ± 1.0

Table 2. Water contact angle hysteresis values measured on zone 1 of treated samples.

Sample	CAH (°)	Std. dev.
1 horizontal	4.54	2.04
2 vertical	1.90	1.50

Table 4. Contact angles with ARNICA 46 for a functionalized sample and an untreated, sandblasted sample.

Sample	CA with ARNICA 46(°)	Std. dev.
UT (sandblasted)	16.7	2.3
2 vertical	123.8	11.8

on the study of the nanocoated slipper with oleophobic properties behavior. Having this in mind, a test bench has been designed at IMAMOTER-C.N.R. in order to assess the behavior of the slippers' surfaces of axial piston pumps.

The complete test bench is depicted in Figure 5.

In order to verify the hydrostatic lubrication working conditions of slippers, it is necessary to know, accurately, the loads and moments acting on the slippers. These are, in an actual pump and motor, difficult to be determined precisely and the behavior of the slippers was, therefore, examined in a hydraulic test bench main data of which are showed in Table 5. The hydraulic diagram of slippers' supply circuit (not completely visible in Figure 5) is showed in Figure 6.

In the usual applications the slipper, connected to the piston, is jointed with the cylinder block and rotates with the drive shaft, while the swash plate is fixed to the pump frame; obviously the swash plate can rotate along an axis orthogonal to the drive shaft. In our test bench, in order to reduce the possible complexities related to the test bench realization (e.g. rotating distributor) but maintaining the relative motion between the slipper and the swash plate, the block cylinder is fixed and the plate rotates. The angle between the plate and the shaft is fixed at 90°.

Knowing the inner (R_1) and outer (R_2) radius of the slipper and the oil pressure (p_o), the force (F) that the slipper exercising on the swash plate can be calculated (Stachowiak and Batchelor 1993).

$$F = p_0 \frac{\pi}{2} \frac{{R_2}^2 - {R_1}^2}{\log \frac{R_2}{R_1}} [N] \tag{1}$$

The resistant torque can be calculated through the following equation:

$$T_r = (L_c \cdot g) \cdot b_r \quad [N \cdot m] \tag{2}$$

where L_c is the load measured by the load cell, g is the gravity acceleration, and b_r is the reaction arm. The friction force can be obtained consequently:

$$F_f = \frac{T_r}{b_f} \quad [N] \tag{3}$$

where b_f is the friction harm which is slightly different with respect to the reaction arm, as reported in Table 5.

Knowing the friction force, the friction coefficient (c_f) can be calculated through the following equation:

$$C_f = \frac{F_f}{F} \tag{4}$$

Table 3. Surface energy (SE) values and its disperse (SE disp) and polar (SE polar) components calculated for zones 1 and 2 of treated samples and of an untreated, sandblasted sample.

Sample	Zone	SE (mN/m)	SE disp (mN/m)	SE polar (mN/m)
UT sandblasted	Zone 1	38.87 ± 1.00	38.54 ± 1.78	0.34 ± 0.01
	Zone 2	36.00 ± 0.50	35.77 ± 2.01	0.23 ± 0.01
1 horizontal	Zone 1	2.28 ± 0.51	2.28 ± 1.00	0
	Zone 2	7.84 ± 1.00	7.47 ± 1.20	0.37 ± 0.01
2 vertical	Zone 1	0.47 ± 0.05	0.46 ± 0.04	0.01 ± 0.01
	Zone 2	7.28 ± 1.00	6.97 ± 1.05	0.31± 0.01

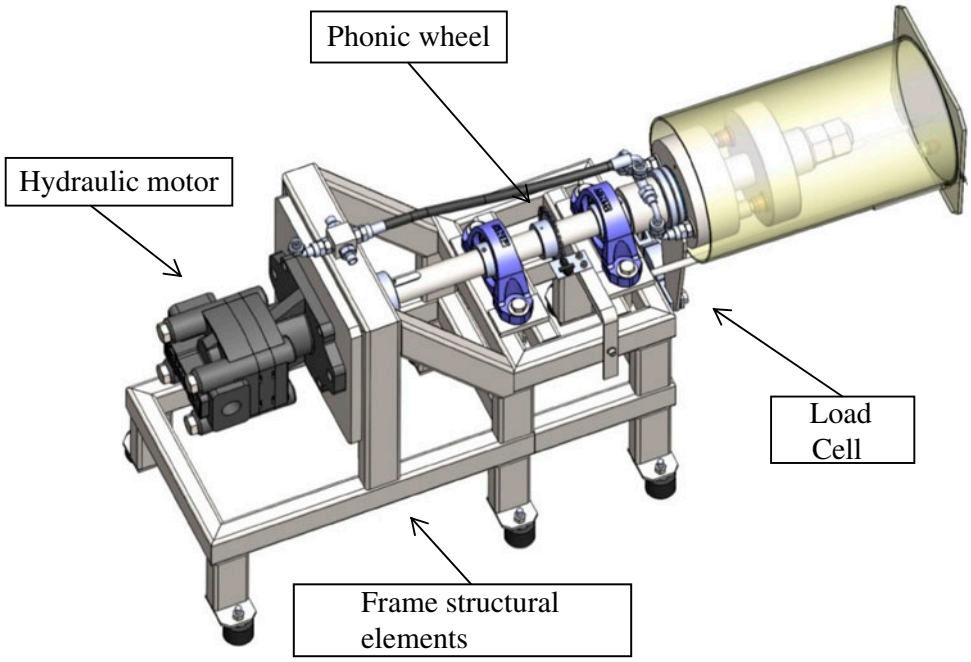

Figure 5. Slippers test bench (the pump of slipper supply circuit is not showed).

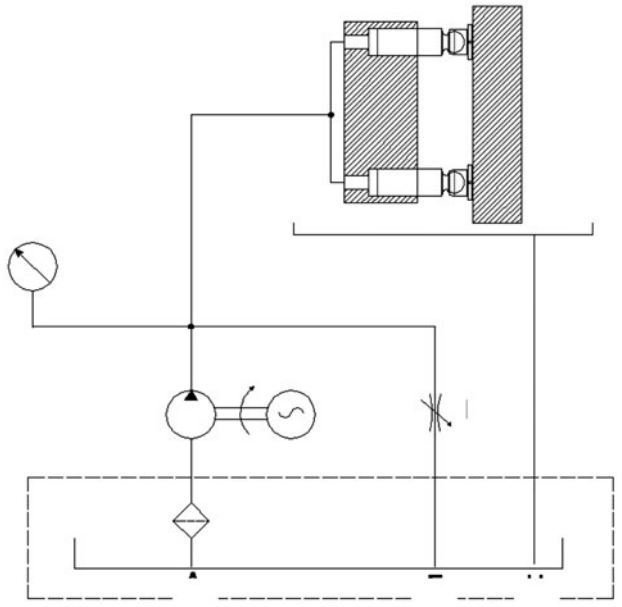

Figure 6. Hydraulic scheme of the cylinder blocks power supply.

Table 5. Test bench data.

Test bench data		
Parameters	Magnitude	Unit
Rotational speed	600–700	rpm
Dynamic load bearing	8100	kg
Reaction arm	0.23	m
Frictional arm	0.15	m
Slipper surface	404.5	mm^2

4.1. Experimental results on standard samples

First of all, the standard samples have been tested on the dedicated test bench in order to have a reference point in terms of friction coefficient. The friction force has been measured using a load cell (*Laumas Electronics, model SA 15*) with a peak value of 15 kg and a combined error of less than ±0.02%. Tables 6 and 7 show the experimental results for standard samples (series 1–2) with a constant rotation velocity (700 rpm) and variable pressure.

The normal force, according to Equation (1), shows a linear relation with the pressure. Also the friction force steps up with the pressure, but more gradually. Considering Equation (4) can be explained why the friction coefficient decreases as the high pressure increases, as showed in Table 7 and Figure 7.

The friction coefficients are displayed graphically in Figure 7. It can be seen as a slight difference between the two series that can be considered as normal results deviation: the tested slippers have been provided by an industrial partner from his normal production.

4.2. Experimental results on functionalized samples

Subsequently the functionalized slippers have been tested in order to assess how the friction coefficient could be influenced by the superoleophobic nanocoating depending on the working pressure. The testing procedure is the same used for the standard sample. To take into consideration the statistical effects, eight pairs of slippers, all functionalized in the same way (vertical dipping), have been tested. In Table 8, the experimental results for functionalized samples are shown.

Table 6. Measured friction force (F_f) and calculated normal force (F) for standard samples.

	Friction force (F_f) – (N)		Normal force (F) – (N)	
Pressure – (bar)	Series 1	Series 2	Series 1	Series 2
10	20.41 ± 1.02	25.99 ± 1.29	406.75	
20	24.97 ± 1.49	35.14 ± 2.44	813.50	
30	29.40 ± 2.05	42.70 ± 1.70	1220.25	
40	33.35 ± 1.33	47.50 ± 2.85	1627.00	
50	37.82 ± 1.51	53.08 ± 2.12	2033.75	

Table 7. Friction coefficient for standard samples.

	Friction coefficient				
Standard samples	10 bar	20 bar	30 bar	40 bar	50 bar
Series 1	0.0502 ± 0.0025	0.0307 ± 0.0018	0.0241 ± 0.0017	0.0205 ± 0.0008	0.0186 ± 0.0007
Series 2	0.0639 ± 0.0032	0.0432 ± 0.0030	0.0350 ± 0.0014	0.0292 ± 0.0018	0.0261 ± 0.0010

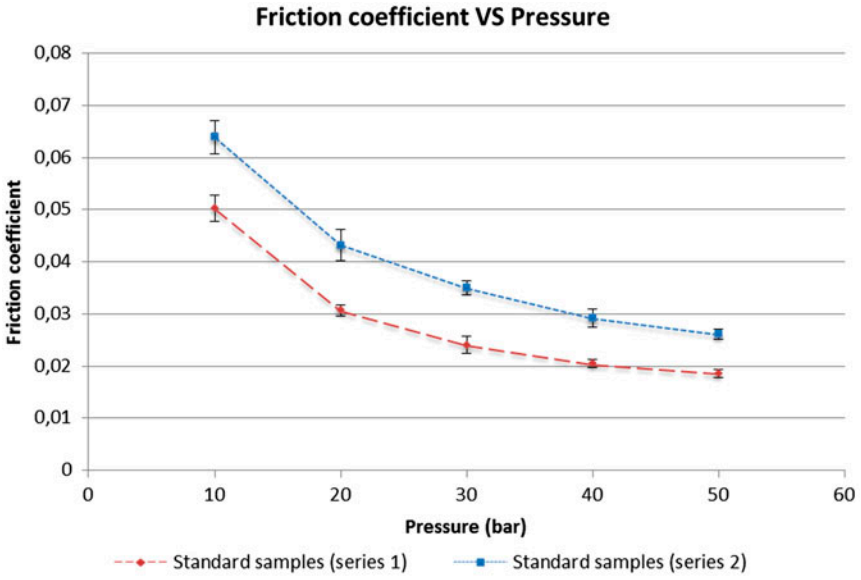

Figure 7. Friction coefficient versus pressure for standard samples.

Table 8. Friction coefficient of functionalized samples.

	Friction coefficient				
Functionalized samples	10 bar	20 bar	30 bar	40 bar	50 bar
Series 1	0.0183 ± 0.0011	0.0149 ± 0.0009	0.0142 ± 0.0007	0.0128 ± 0.0008	0.0120 ± 0.0006
Series 2	0.0183 ± 0.0009	0.0188 ± 0.0008	0.0163 ± 0.0010	0.0142 ± 0.0009	0.0123 ± 0.0005
Series 3	0.0258 ± 0.0011	0.0171 ± 0.0010	0.0151 ± 0.0011	0.0129 ± 0.0008	0.0127 ± 0.0005
Series 4	0.0396 ± 0.0020	0.0199 ± 0.0012	0.0158 ± 0.0007	0.0138 ± 0.0006	0.0128 ± 0.0008
Series 5	0.0302 ± 0.0018	0.0196 ± 0.0010	0.0197 ± 0.0012	0.0176 ± 0.0007	0.0162 ± 0.0010
Series 6	0.0265 ± 0.0016	0.0207 ± 0.0012	0.0173 ± 0.0010	0.0152 ± 0.0008	0.0137 ± 0.0007
Series 7	0.0323 ± 0.0023	0.0168 ± 0.0007	0.0126 ± 0.0008	0.0111 ± 0.0007	0.0103 ± 0.0008
Series 8	0.0364 ± 0.0022	0.0271 ± 0.0014	0.0211 ± 0.0011	0.0179 ± 0.0011	0.0159 ± 0.0006

Table 9. Mean friction coefficient and percentage gain for standard and functionalized samples.

	Mean friction coefficient				
	10 bar	20 bar	30 bar	40 bar	50 bar
Standard samples	0.0570 ± 0.0028	0.0369 ± 0.0024	0.0296 ± 0.0015	0.0249 ± 0.0013	0.0223 ± 0.0009
Functionalized Samples	0.0284 ± 0.0016	0.0194 ± 0.0010	0.0165 ± 0.0009	0.0144 ± 0.0007	0.0132 ± 0.0007
Percentage gain	50.17%	47.56%	44.09%	41.92%	40.74%

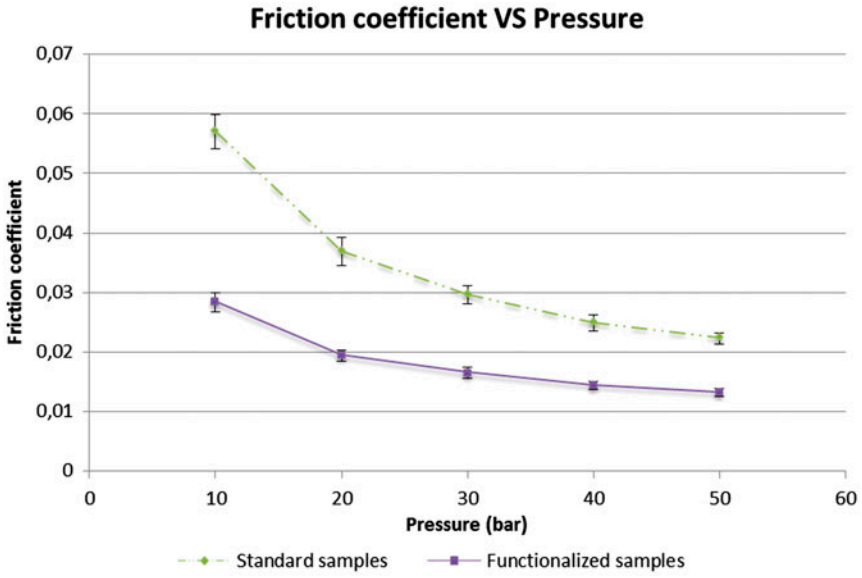

Figure 8. Mean of the friction coefficient versus pressure for standard and functionalized samples.

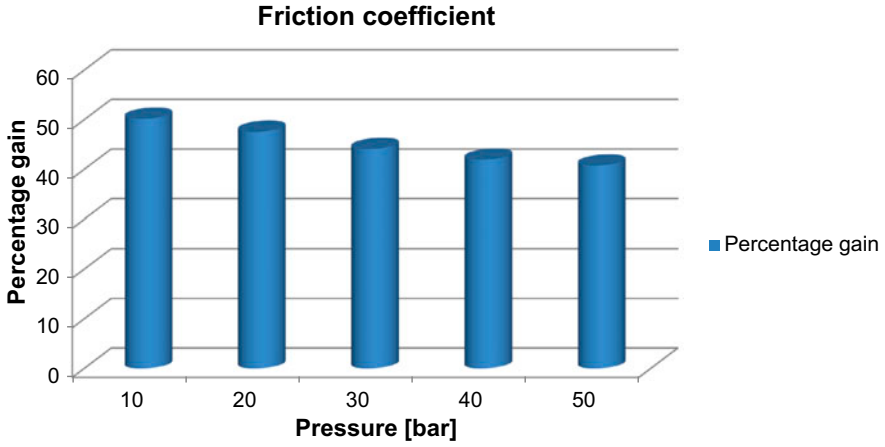

Figure 9. Percentage gain between standard and functionalized samples.

4.3. Comparison between standard and functionalized samples

Using the experimental data shown in Tables 7 and 8 the friction coefficient mean value has been calculated (Table 9) for every working pressure; a comparison between the results can be seen in Figure 8. It clearly shows that the friction coefficient of the functionalized samples is lower than the standard ones. In order to have a clear 'image' of the potential efficiency improvement related to the use of superhydrophobic coating on slipper surface, a percentage gain has been calculated for every working pressure and showed in Figure 9.

5. Conclusions

The application of special nanocoating surface treatments has been exploited by a mixed research team with the aim to reduce the friction losses in a axial piston pump.

A method for the treatment of metallic surface has been developed by ISTEC-C.N.R. and applied in cooperation with IMAMOTER-C.N.R. to the surface of a slipper commonly used in a hydraulic piston pump. To coat the slipper, the dip-coating methodology has been used and a dedicated test bench, able to reproduce the real hydrostatic lubrication working condition, has been designed.

The laboratory studies performed on coated slipper have showed that:

- the coating increases the hydrophobicity of the sample;
- the treatment clearly reduces surface energy (down to values close to zero) with respect to an untreated sample;
- the best performances in terms of high repellence and low surface energy are obtained for a vertical conformation of the sample during dipping;
- the treatment radically modifies the wettability of the sample toward the lubricant oil: from an extremely oleophilic behavior (CA equal to 17°, denoting affinity of the slipper surface for the lubricant) to a quite strong oleophobicity (CA equal to 124°, denoting repellence of the slipper surface toward the lubricant).

The experimental studies performed on a dedicated test bench have showed that:

- all the functionalized sample show a friction coefficient reduction;
- more than 30% of reduction of the friction coefficient can be obtained using the proposed coating methodology;
- a potential improvement of hydraulic piston pump energy efficiency could be obtained using the proposed coating methodology.

Acknowledgement

The authors express their acknowledge to HP S.p.A. (Bondioli & Pavesi Group) for the technical support. The project has been developed under the project *Surface Nano-structured Coating for Improved Performance of Axial Piston Pumps (SNAPP)*, proposed under the "Fabbrica del Futuro" research program, financed by the Italian University and Research Ministry (MIUR) and coordinated by the Italian National Research Council (C.N.R.)

References

Bhushan, B., 2011. Biomimetics inspired surfaces for drag reduction and oleophobicity/philicity. *Beilstein journal of nanotechnology*, 2, 66–84. doi:10.3762/bjnano.2.9

Cassie, A.B. and Baxter, S., 1944. Wettability of porous surfaces. *Transactions of the Faraday Society*, 40, 546–550.

Hooke, C.J., 1989. The lubrication of slippers in axial piston pumps and motors – the effect of tilting couples. *Proceedings of the institution of mechanical engineers, part C: journal of mechanical engineering science*, 203, 343–350.

Iwatsu, R., Hyun, J.M., and Kuwahara, K., 1993. Numerical simulations of three-dimensional flows in a cubic cavity with an oscillating lid. *Journal of fluids engineering*, 115, 680–686.

Kazama, T. and Yamaguchi, A., 1993a. Optimum design of bearing and seal parts for hydraulic equipment. *Wear*, 161 (1–2), 161–171.

Kazama, T. and Yamaguchi, A., 1993b. Application of a mixed lubrication model for hydrostatic thrust bearings of hydraulic equipment. *Journal of tribology*, 115, 686–691.

Kazama, T. and Yamaguchi, A., 1995. Experiment on mixed lubrication of hydrostatic thrust bearings for hydraulic equipment. *Journal of tribology*, 117, 399–402.

Khoo, H.S. and Tseng, F.G., 2008. Engineering the 3D architecture and hydrophobicity of methyltrichlorosilane nanostructures. *Nanotechnology*, 19 (34), 345603. doi:10.1088/0957-4484/19/34/345603

Koc, E., Hooke, C.J., and Li, K.Y., 1992. Slipper balance in axial piston pumps and motors. *Journal of tribology*, 114 (4), 766–772.

Kumar, S., Bergada, J.M., and Watton, J., 2009. Axial piston pump grooved slipper analysis by CFD simulation of three-dimensional NVS equation in cylindrical coordinates. *Computers & fluids*, 38, 648–663. doi:10.1016/j.compfluid.2008.06.007

Li, K.Y. and Hooke, C.J., 1991. Note on the lubrication of composite slippers in water-based axial piston pumps and motors. *Wear*, 147 (2), 413–437.

Li, J., *et al*., 2009. On the measurement of slip length for liquid flow over super-hydrophobic surface. *Chinese science bulletin*, 54, 4560–4565. doi:10.1007/s11434-009-0577-5YU

Liu, K., Yao, X., and Jiang, L., 2010. Recent developments in bio-inspired special wettability. *Chemical society reviews*, 39, 3240–3255. doi:10.1039/b917112f

Ma, W., *et al*., (2012). A "non-sticky" superhydrophobic surface prepared by self-assembly of fluoroalkyl phosphonic acid on a hierarchically micro/nanostructuredalumina gel film. *Chemical communications*, 48, 6824–6826. sol-gel.

Manring, N.D., Wray, C.L., and Dong, Z., 2004. Experimental studies on the performance of slipper bearings within axial-piston pumps. *Journal of tribology*, 126, 511–518.

Martell, Michael B., Rothstein, Jonathan P., and Blair Perot, J., 2010. An analysis of superhydrophobic turbulent drag reduction mechanisms using direct numerical simulation. *Physics of fluids*, 22, 065102. doi:10.1063/1.3432514

Miwa, Masashi, *et al*., 2000. Effects of the surface roughness on sliding angles of water droplets on superhydrophobic surfaces. *Langmuir*, 16, 5754–5760.

Pang, Z., Zhai, W., and Shun, J., 1993. The study of hydrostatic lubrication of the slipper in a high-pressure plunger pump. *Tribology transactions*, 36 (2), 316–320.

Paoluzzi, R., Rigamonti, G., and Zarotti, L.G., 1996. Simulation studies of vehicle-transmission interactions. *Journal of terramechanics*, 33, 143–153.

Raimondo, M., 2012. Making super-hydrophobic building materials: static and dynamic behavior of nanostructured surface. IV ICC4-international ceramic conference, July 14–19 Chicago (USA), Invited talk.

Raimondo, M. and Blosi, M. (ISTEC CNR) and Bezzi, F. and Mingazzini, C. (ENEA UTTMAT Faenza). 2011. Patent 1: RM2011A000104 (deposited in 3 Marzo 2011; PCT procedure is ongoing).

Raimondo, M. and Blosi, M. (ISTEC CNR) and Bezzi, F. and Mingazzini, C. (ENEA UTTMAT Faenza). 2012. Patent 2: RM2012A000291 (depositato in data 21/06/2012).

Raimondo, M., *et al*., 2014. Wetting behavior and remarkable durability of amphiphobic aluminum alloys in a wide range of environmental conditions. *Chemical Engineering Journal*, 258, 101–109. http://dx.doi.org/10.1016/j.cej.2014.07.076

Rothstein Jonathan P., 2010. Slip on superhydrophobic surfaces. Annual review of fluid mechanics, 42, 89–109. doi: 10.1146/annurev-fluid-121108-145558

Stachowiak, G.W. and Batchelor, A.W., 1993. *Engineering tribology.* Amsterdam: Butterworth-Heinemann. ISBN 978-0-12-397047-3.

Tadanaga, K., Katata, N., and Minami, T., 1997. *Journal of the American ceramic society*, 80 (4), 1040–1042.

Tuteja, A., *et al*., 2007. Designing superoleophobic surfaces. *Science*, 318, 1618–1622. doi:10.1126/science.1148326

Wilson, P.W. and Haymet, A.D.J., 2009. Effect of solutes on the heterogeneous nucleation temperature of supercooled water: an experimental determination. *Physical chemistry chemical physics*, 11, 2679–2682. doi:10.1039/B817585C

Wu, Y., *et al*., 2014. Slip flow of diverse liquids on robust superomniphobic surfaces. *Journal of colloid and interface science*, 414, 9–13.

Yao, H., Cooper, R.K., and Raghunathan, S. 2004. Numerical simulation of incompressible laminar flow over three-dimensional rectangular cavities. *Journal of fluids engineering*, 126, 919–927.

Yong, C.J. and Bhushan, B., 2006. Contact angle, adhesion and friction properties of micro- and nanopatterned polymers for superhydrophobicity. *Nanotechnology*, 17, 4970. doi:10.1088/0957-4484/17/19/033

Yu, Yong-Sheng, and Wei, Qing-Ding, 2006. Experimental study on physical mechanism of drag reduction of hydrophobic materials in laminar flow. *Chinese physics letters*, 23 (6), 1634–1637.

Zhou, M., *et al*., 2011. Fluid drag reduction on superhydrophobic surfaces coated with carbon nanotube forests (CNTs). *Soft matter*, 7, 4391–4396. doi:10.1039/C0SM01426E